

Single-Step Phase-Engineered Pulse for Active Readout Cavity Reset in Superconducting Circuits

Ren-Ze Zhao,^{1,2} Ze-An Zhao,^{1,2} Tian-Le Wang,^{1,2} Peng Wang,^{1,2,3} Sheng Zhang,^{1,2,3} Xiao-Yan Yang,^{1,2} Hai-Feng Zhang,^{1,2} Zhi-Fei Li,^{1,2} Yuan Wu,^{1,2} Zi-Hao Fu,^{1,2} Sheng-Ri Liu,^{1,2} Peng Duan,^{1,2,*} and Guo-Ping Guo^{1,2,4,†}

¹Laboratory of Quantum Information, University of Science and Technology of China, Hefei 230026, China

²Synergetic Innovation Center of Quantum Information and Quantum

Physics, University of Science and Technology of China, Hefei 230026, China

³Suzhou Institute for Advanced Research, University of Science and Technology of China, Suzhou, Jiangsu 215123, China

⁴Origin Quantum, Hefei, Anhui 230088, China

(Dated: December 10, 2025)

In a circuit QED architecture, we experimentally demonstrate a simple and hardware-efficient Single-Step Phase-Engineered (SSPE) pulse scheme for actively depopulating the readout cavity. The method appends a reset segment with tailored amplitude and phase to a normal square readout pulse. Within the linear-response regime, the optimal reset amplitude scales proportionally with the readout amplitude, while the optimal reset phase remains nearly invariant, significantly simplifying the calibration process. By characterizing the cavity photons dynamics, we show that the SSPE pulse accelerates photon depletion by up to a factor of six compared to passive free decay. We further quantify the qubit backaction induced by the readout pulse and find that the SSPE pulse yields the lowest excitation and relaxation rates compared to a Square and CLEAR pulses. Our results establish the SSPE scheme as a practical and scalable approach for achieving fast, smooth, low-backaction cavity reset in superconducting quantum circuits.

I. INTRODUCTION

Superconducting qubits realized through circuit quantum electrodynamics [1–4] (QED) have emerged as a leading platform for scalable quantum computation. This architecture has enabled the implementation of high-fidelity two-qubit gates [5, 6], fast and accurate single-shot qubit state readout [6–11], and, notably, the experimental demonstration of quantum error-correction codes have surpassed the fault-tolerance threshold [12–17], marking an essential milestone toward fault-tolerant quantum computing.

A key component of the circuit QED readout scheme is dispersive measurement, wherein the qubit is coupled to a readout resonator cavity. In the dispersive regime, the qubit state induces a frequency shift of the resonator without energy exchange. When the resonator is driven near resonance, its vacuum state is displaced into a qubit-state-dependent coherent state. By demodulating the transmitted or reflected microwave signal, one can infer the qubit state with high fidelity.

For applications requiring mid-circuit measurement [18] and fast feedback [19, 20], it is essential that the readout resonator be rapidly reset following each measurement. Moreover, a variety of qubit reset and leakage removal schemes [21–24] operate by transferring residual qubit excitations into the resonator, thereby converting qubit population into cavity photons that must be promptly depopulated. These considerations underscore the importance of active and

high-performance cavity depopulation techniques in modern superconducting quantum computation.

A straightforward strategy to accelerate resonator reset is to engineer a low-quality-factor readout resonator. However, increasing the resonator linewidth enhances the qubit’s radiative decay through the Purcell effect, thereby degrading lifetime. Although Purcell filters can suppress this decay channel, they typically introduce additional circuit complexity, such as dedicated resonator [9, 25] or bus filter [26, 27]. Pulse-level approaches provide an alternative route to fast cavity depletion without modifying the hardware architecture. In particular, optimal-control techniques have been employed to design tailored drive sequences that efficiently depopulate photons [28]. In the literature [29], two additional segments are appended at the end of the pulse to achieve cavity reset.

In this letter, we present an experimental demonstration of a Single-Step Phase-Engineered (SSPE) active cavity-reset technique that enables smooth and highly efficient photon depletion. Specifically, as illustrated in Fig. 1(a), a reset segment with tailored amplitude and phase is appended to the end of a conventional square readout pulse, yielding a photon-decay rate nearly six times faster than passive free decay. We further characterize the backaction of the reset pulse on qubit, focusing on two dominant sources of non-quantum-nondemolition (non-QND) behavior: qubit excitation and relaxation errors. Our results show that our SSPE pulse outperforms the conventional square pulse and CLEAR [29] pulse, achieving significantly lower excitation rates and reduced relaxation rates.

* pengduan@ustc.edu.cn

† gpguo@ustc.edu.cn

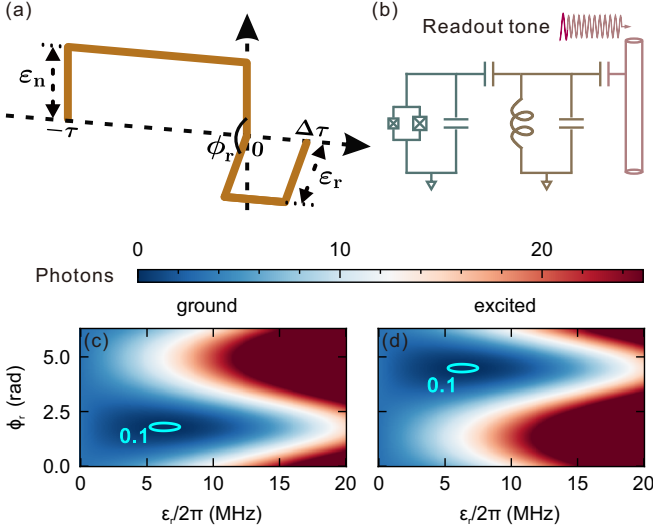


FIG. 1. **Structure and Performance of the SSPE Pulse.** (a) Schematic of the SSPE pulse, which consists of two segments: a normal readout segment with drive amplitude ε_n and phase ϕ_n , followed by a reset segment with drive amplitude ε_r and phase ϕ_r . (b) Equivalent lumped-element circuit model. (c), (d) Residual photon number at the end of the SSPE pulse as a function of the reset amplitude and phase for the qubit prepared in $|0\rangle$ and $|1\rangle$, respectively. A residual photon number of zero indicates that the cavity field has returned to vacuum, corresponding to complete photon dissipation. Light cyan contours denote the photon number level of 0.1.

II. THEORETICAL MODEL

In a circuit QED architecture, a superconducting qubit is coupled to a superconducting resonator cavity, typically implemented as a quarter-wavelength ($\lambda/4$) coplanar waveguide transmission line [30]. This system can be modeled by an equivalent lumped-element circuit in which the qubit is capacitively coupled to a linear LC oscillator, as illustrated schematically in Fig. 1(b). When a microwave pulse with a frequency near resonance is injected into the input port, the cavity field evolves into a coherent field. The dynamics of coherent field amplitude $\alpha(t)$ can be obtained from input-output theory [31–33], and can be shaped through appropriate engineering of the drive envelope. The resulting dynamics are governed by the differential equation [1, 34]

$$\dot{\alpha}_j(t) = -i\varepsilon_d(t) - i(\Delta_r + \chi_j)\alpha_j(t) - \frac{\kappa}{2}\alpha_j(t), \quad (1)$$

with $\Delta_r = \omega_r - \omega_d$ denotes the detuning between the bare cavity frequency ω_r and the cavity drive frequency ω_d . $\varepsilon_d(t)$ represents the (generally complex) time-dependent amplitude of the external drive. κ is cavity decay rate. χ_j denotes the dispersive shift of the cavity resonance frequency associated with the qubit being in state $|j\rangle$, where $j = 0, 1, \dots$ corresponds to the ground, first excited, and higher excited states, respectively. For $j > 0$

$$\begin{aligned} \chi_j &= \chi_{j-1,j} - \chi_{j,j+1}, \\ \chi_{j-1,j} &= \frac{Jg^2}{\Delta + (j-1)\eta}, \end{aligned} \quad (2)$$

particularly, $\chi_0 = -g^2/\Delta$, where g is the qubit-cavity coupling strength, η is qubit anharmonicity, and $\Delta = \omega_q - \omega_r$ is the detuning between the qubit frequency ω_q and the bare cavity frequency. In this work, we restrict our analysis to the cavity-reset dynamics for the qubit is in either $|0\rangle$ or $|1\rangle$. The instantaneous mean intracavity photon number is given by

$$\bar{n}_j(t) = |\alpha_j(t)|^2. \quad (3)$$

We emphasize that our SSPE pulse is constructed from piecewise complex constant amplitudes and consists of two segments: a normal readout segment of duration τ with drive amplitude ε_n and phase ϕ_n , followed by a reset segment of duration $\Delta\tau$ with amplitude ε_r and phase ϕ_r .

$$\varepsilon_d(t) = \begin{cases} \varepsilon_n e^{i\phi_n}, & -\tau \leq t < 0, \\ \varepsilon_r e^{i\phi_r}, & 0 \leq t \leq \Delta\tau, \end{cases} \quad (4)$$

Throughout this work, both ε_n and ε_r are taken to be real. The relative phase $\Delta\phi = \phi_r - \phi_n$, determines the dynamics of the cavity coherent field and plays a crucial role in determining the reset power. Assuming $\phi_n = 0$, this reduces to $\Delta\phi = \phi_r$.

Under the drive of this piecewise constant pulse, the coherent field amplitude $\alpha_j(t)$ evolves accordingly

$$\alpha_j(t) = \begin{cases} \frac{2\varepsilon_n(-1 + e^{-\frac{1}{2}(t+\tau)C_j})}{-iC_j}, & -\tau \leq t < 0, \\ 2e^{-\frac{1}{2}tC_j} \times \frac{\varepsilon_r e^{i\phi_r}(1 - e^{\frac{1}{2}tC_j}) - \varepsilon_n(1 - e^{-\frac{1}{2}\tau C_j})}{-iC_j}, & 0 \leq t \leq \Delta\tau, \end{cases} \quad (5)$$

where $C_j = 2i\Delta_r + \kappa + 2i\chi_j$. For a fixed readout amplitude ε_n and duration τ , typically optimized for high readout fidelity, and for a chosen reset duration $\Delta\tau$, one can always identify a pair of reset parameters (ε_r, ϕ_r) that returns the cavity field to vacuum state at the end of the pulse, i.e

$$|\alpha_j(\Delta\tau)|^2 = 0, \quad (6)$$

this condition can be satisfied for both qubit states $|0\rangle$ and $|1\rangle$, as demonstrated in Fig. 1(c) and 1(d). Although the exact analytical forms of the optimal reset parameters are cumbersome due to the nontrivial driven dynamics of the cavity, they can be obtained efficiently through

simple numerical optimization. In principle, cavity reset can be performed in an arbitrarily short time. In practice, however, the achievable depletion rate is limited by the maximum drive amplitude available from the control hardware. Furthermore, we emphasize a key feature of our scheme: when the readout amplitude is rescaled, the corresponding optimal reset amplitude scales proportionally, while the optimal reset phase remains invariant. This scaling behavior substantially simplifies calibration procedures and will be further demonstrated in the following sections.

III. EXPERIMENTAL RESULTS

The experimental qubit is a frequency-tunable transmon [35] with frequency $\omega_q/2\pi = 5445.786$ MHz at sweet spot, anharmonicity $\eta/2\pi = -216.7447$ MHz, average $T_1 = 31.473$ μ s and average Hahn-echo coherence time $T_2^{\text{echo}} = 45.566$ μ s. The bare cavity resonance frequency is measured to be $\omega_{\text{bare}}/2\pi = 7123.9$ MHz. When the transmon is prepared in $|0\rangle$, the dressed cavity frequency shifts to $\omega_{|0\rangle}/2\pi = 7139.389$ MHz, preparing in the $|1\rangle$ results in a dispersive shift of $2\chi/2\pi = -3.861$ MHz. The cavity decay rate is $\kappa/2\pi = 1.711$ MHz, corresponding to a photon lifetime of $T_{\text{cav}} = 1/\kappa = 93$ ns. In the dispersive regime, the critical photon number is approximately given by $n_{\text{crit}} = \Delta^2/4g^2$ [1]. As the intracavity photon number approaches n_{crit} , nonlinear effects become non-negligible [36–38], and the cavity response exhibits state-dependent nonlinearity. Throughout this work, the cavity drive frequency is set to be the average of the dressed cavity frequencies associated with the qubit states $|0\rangle$ and $|1\rangle$. Further experimental setup details are provided in Appendix A.

In this letter, we fix the duration of the reset segment to $\Delta\tau = 50$ ns $\approx T_{\text{cav}}/2$. After determining the optimal reset parameters (ε_r, ϕ_r) , we quantify the power of the cavity reset by measuring the residual photon number at a time t_{relax} following the end of readout pulse. To extract this quantity, we employ a Ramsey-based technique used in the literature [29] to capture photon-induced dephasing and frequency shift. The resulting Ramsey trace is fitted to the functional form

$$S(t) = \frac{1}{2} [1 - \text{Im} \{ \exp [-(\Gamma_2 + \Delta\omega i)t + (\phi_0 - 2n_0\chi Z)i] \}], \quad (7)$$

where $\Delta\omega$ is Ramsey fringe, and $\Gamma_2 = 1/T_2^{\text{echo}}$ is decoherence rate. $Z = (1 - e^{-(\kappa + 2\chi i)t}) / (\kappa + 2\chi i)$, ϕ_0 is a fit offset phase, n_0 represents the photon number at time t_{relax} .

For a fair comparison, we compare the residual population following the SSPE pulse and Square pulse with an extra delay time $\Delta\tau$ for passive free decay, to ensure that both schemes have equal total duration. The measured results are shown in Fig. 2(a). Across the full range of applied normal readout segment drive amplitudes which are parameterized by the scaling factor $\beta_n = \varepsilon_n/\varepsilon_n$ (set by

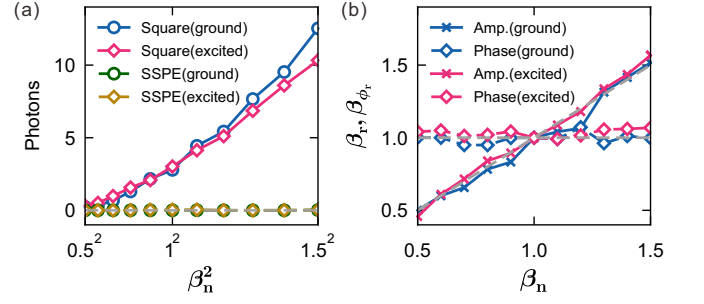


FIG. 2. **Residual Photon Population and Parameter Scaling of the SSPE Pulse.** (a) Residual photon population as a function of the drive amplitude, measured either at a delay of $\Delta\tau = 50$ ns following the end of a Square pulse or immediately after the SSPE pulse. The drive amplitude is parameterized by the scale factor β_n defined in the main text, where $\beta_n = 1$ corresponds to the calibrated readout amplitude that yields high readout fidelity. (b) Scaling behavior of the optimal reset parameters. The rescaling factors for the optimal reset amplitude and reset phase, extracted for each value of the rescaled readout amplitude β_n , are plotted as a function of β_n . Gray dashed lines denote the reference lines $y = 1$ and $y = x$.

the applied DAC voltage, with the voltage-to-photon calibration provided in Appendix C), our SSPE pulse consistently suppresses the residual photon population to zero, demonstrating highly efficient cavity depopulation. In contrast, the Square pulse exhibits a residual photon population that increases linearly with the square of drive amplitude, consistent with the cavity's linear-response behavior. As the drive amplitude increases further, however, nonlinear effects become apparent. The cavity frequency acquires a photon-number dependence, leading to state-dependent residual photon populations. These deviations indicate the onset of state-dependent cavity nonlinear response and degrade the performance of reset protocols that do not explicitly compensate for such effects. The robustness of our SSPE pulse against these effects highlights its suitability for use in both the linear and weakly nonlinear regimes.

We further emphasize that the proposed SSPE reset scheme exhibits remarkably favorable and experimentally convenient scaling behavior. When the amplitude of the normal readout segment is rescaled by a factor β_n , the corresponding optimal reset amplitude rescales proportionally $\varepsilon'_r = \beta_r \varepsilon_r$, with $\beta_r = \beta_n$. In contrast, the optimal reset phase is invariant under this rescaling, $\beta_{\phi_r} = \phi'_r/\phi_r = 1$. This linear-amplitude but fixed-phase scaling behavior, summarized in Fig. 2(b), significantly simplifies the calibration procedure. Once the optimal reset phase is determined, it can be reused for any readout amplitude, while the reset amplitude can be obtained through simple proportional scaling.

Fig. 3(a–c) display the trajectories of the cavity field in the in-phase-quadrature (IQ) plane during the reset segment for the SSPE, CLEAR and Square pulse (free

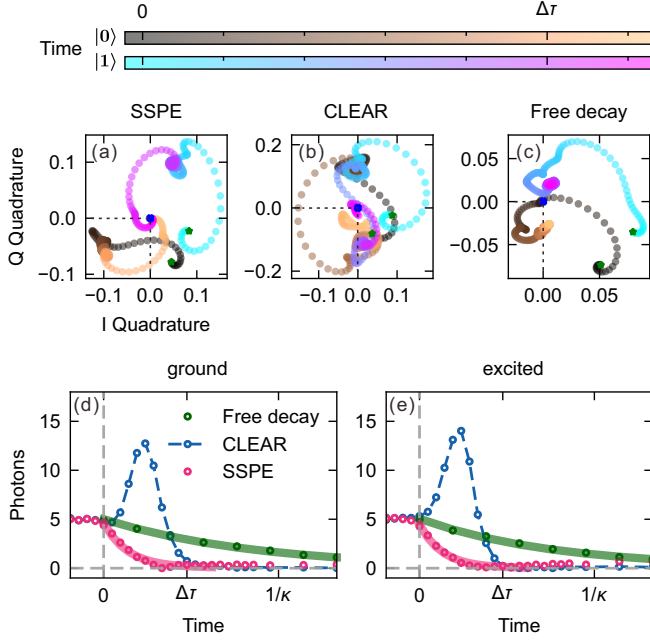


FIG. 3. **Cavity Reset Dynamics.** (a-c) IQ-plane trajectories of the cavity field during the reset interval for the SSPE pulse, CLEAR pulse, and free decay, respectively. In each panel, the blue cross marks the origin, and the green stars denotes the initial point of the trajectory. The colorbars represent the time index, with the "copper" colormap (top) and "cool" colormap (bottom) corresponding to the qubit in $|0\rangle$ and $|1\rangle$, respectively. (d), (e) Photon reset dynamics for the three different reset schemes. The full time-resolved dynamics are provided in Appendix B. The green and red curves correspond to exponential fits for the free-decay and SSPE pulse reset processes, respectively.

decay), respectively. To ensure a consistent and fair comparison, the durations of the reset segments in the SSPE and CLEAR pulses, as well as the passive free-decay interval following the Square pulse, are chosen to be identical. Both the SSPE and CLEAR pulses steer the cavity field back to the origin of the IQ plane by the end of the reset segment, demonstrating complete depletion of the residual photons. In contrast, the Square pulse, which relies solely on passive free decay, fails to return the cavity field to the vacuum state within the same time duration.

To characterize the photon dynamics during cavity reset, we employ the pulse sequence described in Appendix B. A calibrated qubit π -pulse is frequency-swept to measure the photon-induced ac-Stark shift [39], $\Delta\omega_q = 2\chi n$, where n denotes the mean intracavity photon number. By varying the delay of the π -pulse, we obtain time-resolved measurements of $n(t)$. Fig. 3(d) and 3(e) show the measured photon dynamics for the three reset protocols with the qubit initialized in $|0\rangle$ and $|1\rangle$, respectively. For the Square pulse, the photon population follows a standard exponential decay, with fitted decay rates of $\kappa_{|0\rangle}/2\pi = 1.711$ MHz and $\kappa_{|1\rangle}/2\pi = 1.984$ MHz. In contrast, the SSPE pulse drives the cavity population

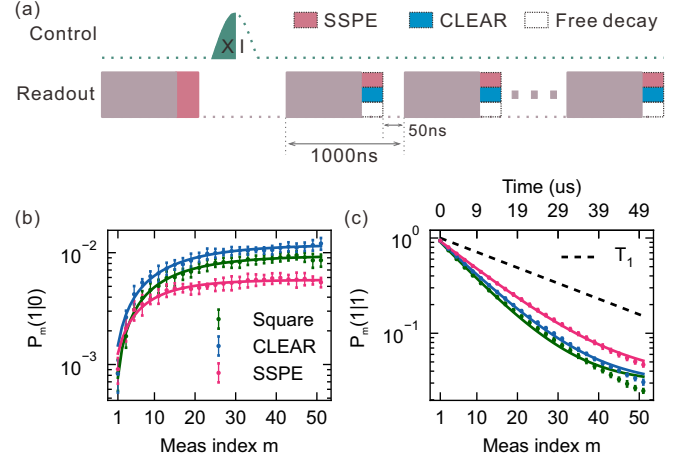


FIG. 4. **Qubit Backaction Characterization.** (a) Experimental pulse sequence employed to characterize measurement-induced backaction on the qubit. A SSPE pulse is first applied as a pre-measurement to ensure the qubit is initialized in $|0\rangle$. The qubit is then prepared in either $|0\rangle$ or $|1\rangle$, followed by repeated measurements using one of three reset schemes: SSPE (red), CLEAR (blue), and Square (free decay, unfilled). (b) Probability $P_m(1|0)$ for the qubit prepared in $|0\rangle$. (c) Probability $P_m(1|1)$ for the qubit prepared in $|1\rangle$. The black dashed line denotes the intrinsic relaxation expected from $T_1 = 26.51 \mu s$ at the photon-induced ac-Stark-shifted qubit frequency under the steady-state readout photon number. The experimental data points in panels (b) and (c) are plotted by sampling every two measurement cycles.

rapidly and smoothly to near-zero levels. Exponential fits yield decay rates of $\kappa_{|0\rangle}^{\text{SSPE}}/2\pi = 10.968$ MHz and $\kappa_{|1\rangle}^{\text{SSPE}}/2\pi = 11.618$ MHz, approximately six times faster than passive decay. The CLEAR pulse likewise returns the cavity to vacuum, but its trajectory exhibits a pronounced overshoot in photon number prior to depletion. This transient increase in cavity population can enhance measurement-induced backaction on the qubit, a consequence that we examine in detail in the following section.

It is essential to quantify the measurement-induced backaction on the qubit. Spurious qubit excitation [40–46] and relaxation [47–49] induced by the readout pulse are well-documented phenomena in dispersive measurements of superconducting qubits. We characterize these effects using the pulse sequence shown in Fig. 4(a). The sequence begins with a pre-measurement SSPE pulse, which resets the cavity and initializes the transmon in the ground state $|0\rangle$. Following initialization, the transmon is prepared in either $|0\rangle$ or $|1\rangle$, and subsequently subjected to repeated measurements using one of the three readout pulses. The interval between adjacent measurement pulses is fixed at 50 ns, and each pulse has a duration of 950 ns, yielding a total separation of $\Delta t = 1 \mu s$ between successive measurements. Fig. 4(b) and 4(c) show the measured probabilities $P_m(1|0)$ and $P_m(1|1)$, where $P_m(i|j)$ denotes the probability of finding the qubit in state $|i\rangle$ during the m -th measurement given initializa-

tion in state $|j\rangle$. The evolution of these probabilities under repeated measurements is well described by the phenomenological model [50]

$$P_m = C(1 - \gamma_o - \gamma_b)^{(m-1)} + P_{m \rightarrow \infty}, \quad (8)$$

where $P_{m \rightarrow \infty} = \gamma_b / (\gamma_o + \gamma_b)$ represents the steady-state probability and $C = P_0 - P_{m \rightarrow \infty}$ is determined by the initial condition. The exponent $m - 1$ reflects that the measurement index begins at $m = 1$. Here, γ_o and γ_b are transition rate, denote the transition probabilities out of and back into the initial state per measurement, respectively.

For a transmon qubit, higher excited states ($|2\rangle$ and above) yield IQ responses that lie closer to that of $|1\rangle$ [40, 41, 46, 51]. When the transmon is initialized in $|0\rangle$, γ_o predominantly captures excitation out of $|0\rangle$, and γ_b characterizes relaxation back into $|0\rangle$. As illustrated in Fig. 4(b), our SSPE pulse exhibits the minimum excitation rate, 0.05%. Conversely, when the transmon is initialized in $|1\rangle$, γ_o primarily captures relaxation to $|0\rangle$, while γ_b accounts for excitation back into $|1\rangle$ or transitions to higher excited states. As shown in Fig. 4(c), all the three pulses produce enhanced relaxation relative to the intrinsic decay rate, estimated as $1 - e^{-\Delta t/T_1} = 3.7\%$ at the photon-induced ac-Stark-shifted frequency. The Square pulse produces the maximum relaxation rate, 9.54%, whereas the SSPE pulse yields the minimum value, 7.22%. These observations are consistent with the photon dynamics shown in Fig. 3(e), where the Square and SSPE pulses exhibit the maximum and minimum average intracavity photon populations during the reset interval, respectively. Among all protocols tested, the SSPE pulse minimizes both erroneous excitation and relaxation, demonstrating its effectiveness in suppressing measurement-induced backaction and in preserving qubit-state fidelity under repeated readout operations.

IV. CONCLUSION AND OUTLOOK

In summary, we have introduced a simple and effective SSPE pulse scheme that enables active cavity reset in circuit QED systems. By appending a reset segment with tailored amplitude and phase to a conventional square readout pulse, the approach achieves rapid and smooth photon depletion without requiring additional hardware. The reset amplitude scales proportionally with the readout amplitude, while the optimal reset phase remains invariant, substantially reducing calibration overhead. Compared with Square and CLEAR pulses, the proposed protocol consistently suppresses spurious qubit excitation and relaxation, thereby mitigating measurement-induced backaction. This SSPE scheme provides a practical approach for controlling the photon-induced ac-Stark dynamics and offers a versatile tool for investigating non-QND effects associated with the readout process [52]. It

is also well suited for integration into mid-circuit measurement and fast-feedback operations. Future directions include designing time-dependent amplitude and phase profiles to realize qubit-state-independent cavity reset, optimizing the reset segment simultaneously enhance photon depletion and readout fidelity under fixed-duration constraints, and extending the method to multi-qubit architectures that share a common readout resonator.

ACKNOWLEDGMENTS

This work is supported by the National Natural Science Foundation of China (Grant No. 12404564). This work is also partially carried out at the USTC Center for Micro and Nanoscale Research and Fabrication.

DATA AVAILABILITY

The data that support the findings of this article are not publicly available. The data are available from the authors upon reasonable request.

Appendix A: Experimental Setup

Our experiments are carried out on a tunable-coupling superconducting quantum processor consisting of a minimal coupling unit formed by two transmon qubits and a central tunable coupler. Both the qubits and the coupler employ asymmetric superconducting quantum interference device (SQUID) loops, providing frequency tunability via externally applied magnetic flux. Each qubit is equipped with dedicated control and measurement hardware, including an independent XY control line for implementing single-qubit rotations, a Z control line for flux tuning, and an individual dispersive readout resonator. The relevant device parameters are summarized in Table I.

The quantum processor is installed at the mixing chamber (MC) stage of a dilution refrigerator operating at a base temperature of approximately 20 mK. Signal delivery and readout are facilitated by a cryogenic wiring network incorporating multiple stages of attenuation and filtering to mitigate thermal and technical noise. Flux control is generated using an arbitrary waveform generator (AWG) with a sampling rate of 1.2 GSa/s, enabling both static flux biasing and fast flux-pulse operation. Qubit drive and readout signals are synthesized using a radio-frequency (RF) module covering 3.75–8.25 GHz with a sampling rate of 3.2 GSa/s. Dispersive readout is performed in transmission: signals produced by mixing DAC outputs with a local-oscillator (LO) tone propagate through an impedance-matched parametric amplifier (IMPA) [53] located at the MC stage and a high-electron-mobility transistor (HEMT) amplifier at 4 K.

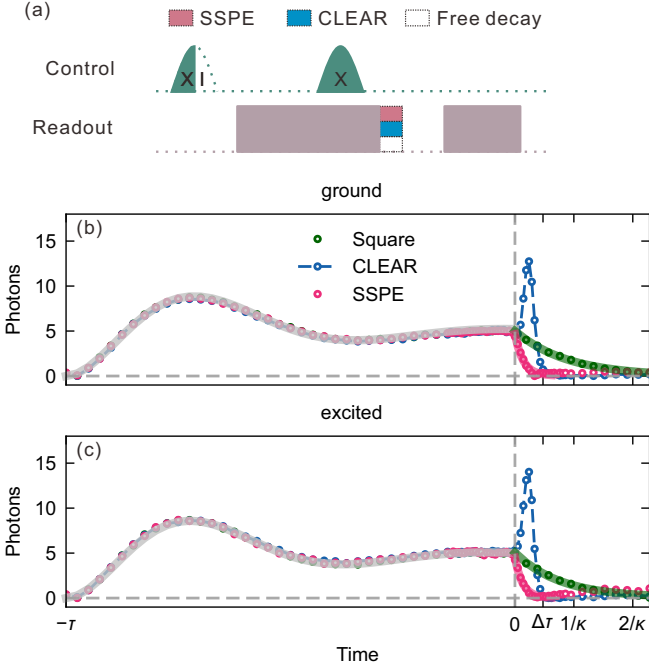


FIG. 5. **Time-Resolved Characterization of Cavity Photon Dynamics.** (a) Experimental pulse sequence used to characterize photon dynamics. The qubit is prepared in either $|0\rangle$ or $|1\rangle$, followed by a frequency-swept calibrated qubit π -pulse to measure the photon-induced ac-Stark shift. A final square readout pulse is then used to perform high-fidelity qubit state discrimination. The delay between the two readout pulses is set to 300 ns (500 ns) for SSPE and CLEAR pulse (Square pulse), ensuring that residual photons have fully depleted prior to the second measurement. (b), (c) Time-resolved measurements of the intracavity photon number for the qubit prepared in $|0\rangle$ and $|1\rangle$, respectively. Light gray curves correspond to fits obtained from the nonlinear cavity dynamics model described by Eq. (B.1).

Subsequent room-temperature amplification and down-conversion to an intermediate frequency (IF) precede digitization and demodulation, after which the extracted in-phase (I) and quadrature (Q) components are used for high-fidelity quantum-state discrimination.

Appendix B: The Dynamics of Photons

To characterize the photon dynamics, we employ the pulse sequence depicted in Fig. 5(a). The qubit is prepared in either $|0\rangle$ or $|1\rangle$, after which a calibrated qubit π -pulse is frequency-swept to measure the photon-induced ac-Stark shift [39], $\Delta\omega_q = 2\chi n$. The resulting shift in the qubit transition frequency provides a direct estimate of the mean intracavity photon number n . By varying the delay of the π -pulse, we obtain a time-resolved reconstruction of $n(t)$, as shown in Fig. 5(b) and 5(c). During the readout segment, the cavity may enter a weakly nonlinear regime, particularly at high drive powers. To

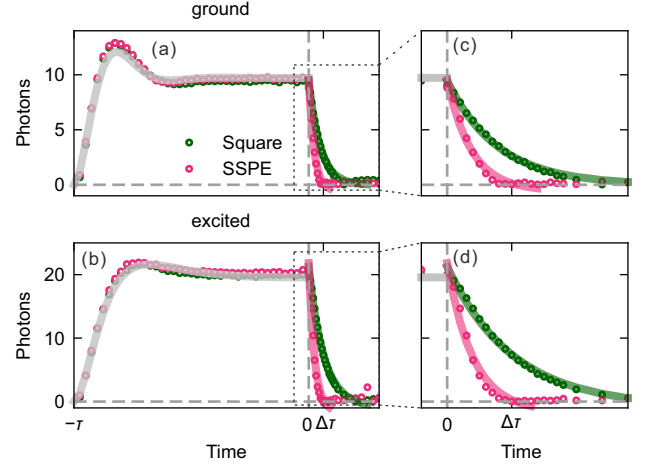


FIG. 6. **Cavity Photon Dynamics.** (a), (b) Time-resolved measurements of intracavity photon number for qubit Q2 prepared in $|0\rangle$ or $|1\rangle$, respectively. Light gray lines denote fits obtained from the nonlinear equation of motion described by Eq. (B.1). Exponential fits to the photon decay under the Square (free-decay) pulse are shown in green, yielding decay rates of $\kappa_{|0\rangle}/2\pi = 4.054$ MHz and $\kappa_{|1\rangle}/2\pi = 3.127$ MHz. Corresponding fits for the SSPE pulse are shown in red, with extracted decay rates of $\kappa_{|0\rangle}^{\text{SSPE}}/2\pi = 8.499$ MHz and $\kappa_{|1\rangle}^{\text{SSPE}}/2\pi = 8.043$ MHz. (c), (d) Expanded views of the reset segments from panels (a) and (b), illustrating the enhanced photon depletion achieved with the SSPE pulse for both qubit states.

accurately capture this behavior, the evolution of the coherent field $\alpha(t)$ is modeled using a nonlinear equation of motion that incorporates the Kerr nonlinearity [52]

$$\begin{aligned} \dot{\alpha}_j(t) = & -i\varepsilon_d(t) - i(\Delta_r + \chi_j)\alpha_j(t) \\ & - iK_c|\alpha_j(t)|^2\alpha_j(t) - \frac{\kappa}{2}\alpha_j(t), \end{aligned} \quad (\text{B.1})$$

here K_c is Kerr coefficient of cavity. The nonlinear term $iK_c|\alpha_j(t)|^2\alpha_j(t)$ accounts for the photon-number-dependent renormalization of the cavity resonance frequency, producing an frequency shift of $K_cn_j(t)$, where $n_j(t) = |\alpha_j(t)|^2$ is the instantaneous intracavity photon number.

For completeness, we extend our characterization of the photon dynamics and cavity-reset performance to a second, nominally identical transmon qubit (Q2). The corresponding results are presented in Fig. 6, and the relevant device parameters for Q2 are summarized in Table I.

Appendix C: The Voltage-to-photon Calibration

To further characterize the cavity response, we calibrate the intracavity photon number as a function of the applied DAC voltage, as shown in Fig. 7. In this procedure, the first pulse in Fig. 5(a) is replaced by a square readout pulse of sufficiently long duration (approximately

TABLE I. Device parameters

Device Parameters	Q_1	Q_2
Qubit 0-1 transition frequency $\omega_q/2\pi$ (MHz)	5445.786	5512.566
Qubit anharmonicity $\eta/2\pi$ (MHz)	-216.744	-218.93
T_1 at sweep spot (μs)	31.473	22.502
T_1 at photon-induced ac-Stark-shifted frequency (μs)	26.51	19.847
T_2^* at sweep spot (μs)	19.716	21.119
T_2^{echo} at sweep spot (μs)	45.566	28.723
Bare cavity frequency $\omega_{\text{bare}}/2\pi$ (MHz)	7123.9	7103.79
Cavity frequency when qubit in $ 0\rangle$ $\omega_{ 0\rangle}/2\pi$ (MHz)	7139.389	7116.255
Dispersive shift $(\omega_{ 1\rangle} - \omega_{ 0\rangle})/2\pi$ (MHz)	-3.861	-4.435
Cavity decay rate when qubit in $ 0\rangle$ (MHz)	1.711	4.054
Cavity decay rate when qubit in $ 1\rangle$ (MHz)	1.984	3.127
Readout duration (ns)	900	900
Reset duration (ns)	50	50
Qubit-Cavity coupling strength $g/2\pi$ (MHz)	147.14	150.465

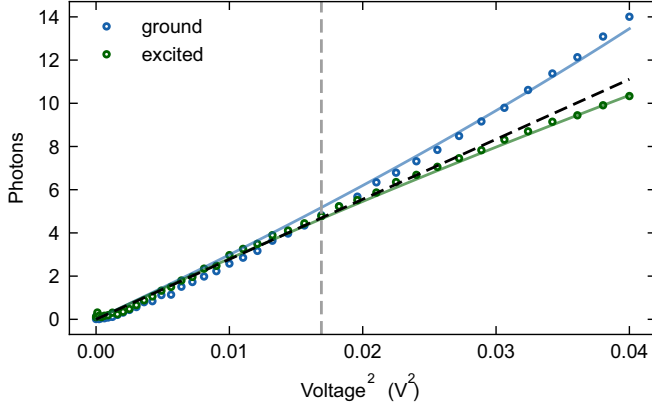


FIG. 7. **Calibration of Intracavity Photon Number Versus DAC Voltage.** Intracavity photon number as a function of the squared DAC voltage. At elevated drive amplitudes, cavity nonlinearities give rise to state-dependent deviations in the photon population for a fixed drive amplitude. The black dashed line denotes the expected linear-response behavior of the cavity.

$25/\kappa$) to ensure that the cavity field reaches its steady state. A calibrated 100 ns π -pulse is applied at the end of the long pulse to achieve enhanced frequency resolution, while the DAC voltage is swept to vary the drive amplitude. By fitting the resulting data to the nonlinear cavity dynamics described by Eq. (B.1), we extract a Kerr coefficient of $K_c/2\pi = -11$ kHz.

- [1] A. Blais, A. L. Grimsmo, S. M. Girvin, and A. Wallraff, Circuit quantum electrodynamics, *Rev. Mod. Phys.* **93**, 025005 (2021).
- [2] A. Blais, R.-S. Huang, A. Wallraff, S. M. Girvin, and R. J. Schoelkopf, Cavity quantum electrodynamics for superconducting electrical circuits: An architecture for quantum computation, *Phys. Rev. A* **69**, 062320 (2004).
- [3] A. Blais, J. Gambetta, A. Wallraff, D. I. Schuster, S. M. Girvin, M. H. Devoret, and R. J. Schoelkopf, Quantum-information processing with circuit quantum electrodynamics, *Phys. Rev. A* **75**, 032329 (2007).
- [4] P. Krantz, M. Kjaergaard, F. Yan, T. P. Orlando, S. Gustavsson, and W. D. Oliver, A quantum engineer's guide to superconducting qubits, *Applied Physics Reviews* **6**, 021318 (2019).
- [5] R. Li, K. Kubo, Y. Ho, Z. Yan, Y. Nakamura, and H. Goto, Realization of high-fidelity cz gate based on a double-transmon coupler, *Phys. Rev. X* **14**, 041050 (2024).
- [6] F. Marxer, J. Mrozek, J. Andersson, L. Abdurakhimov, J. Adam, V. Bergholm, R. Beriwal, C. F. Chan, S. Dahl, S. R. Das, F. Deppe, O. Fedorets, *et al.*, *Above 99.9 fidelity single-qubit gates, two-qubit gates, and readout in a single superconducting quantum device* (2025), [arXiv:2508.16437 \[quant-ph\]](https://arxiv.org/abs/2508.16437).
- [7] L. Chen, H.-X. Li, Y. Lu, C. W. Warren, C. J. Krizan, S. Kosen, M. Rommel, S. Ahmed, A. Osman, J. Biznárová, A. Fadavi Roudsari, B. Lienhard, M. Caputo, K. Grigoras, L. Grönberg, J. Govenius, A. F. Kockum, P. Delsing, J. Bylander, and G. Tancredi,

- Transmon qubit readout fidelity at the threshold for quantum error correction without a quantum-limited amplifier, *npj Quantum Information* **9**, 26 (2023).
- [8] F. m. c. Swiadek, R. Shillito, P. Magnard, A. Remm, C. Hellings, N. Lacroix, Q. Ficheux, D. C. Zanuz, G. J. Norris, A. Blais, S. Krinner, and A. Wallraff, Enhancing dispersive readout of superconducting qubits through dynamic control of the dispersive shift: Experiment and theory, *PRX Quantum* **5**, 040326 (2024).
 - [9] P. A. Spring, L. Milanovic, Y. Sunada, S. Wang, A. F. van Loo, S. Tamate, and Y. Nakamura, Fast multiplexed superconducting-qubit readout with intrinsic purcell filtering using a multiconductor transmission line, *PRX Quantum* **6**, 020345 (2025).
 - [10] C. Wang, F.-M. Liu, H. Chen, Y.-F. Du, C. Ying, J.-W. Wang, Y.-H. Huo, C.-Z. Peng, X. Zhu, M.-C. Chen, C.-Y. Lu, and J.-W. Pan, Longitudinal and nonlinear coupling for high-fidelity readout of a superconducting qubit, *Phys. Rev. Lett.* **135**, 060803 (2025).
 - [11] Y. Xiong, Z. Wang, J. Zhang, X. Sun, Z. Zhang, P. Huang, Y. Liang, J. Jiang, J. Qiu, Y. Zhou, X. Linpeng, W. Huang, J. Niu, Y. Zhong, J. Chu, S. Liu, and D. Yu, High-performance multiplexed readout of superconducting qubits with a tunable broadband purcell filter (2025), [arXiv:2509.11822 \[quant-ph\]](https://arxiv.org/abs/2509.11822).
 - [12] Google Quantum AI, Suppressing quantum errors by scaling a surface code logical qubit, *Nature* **614**, 676 (2023).
 - [13] Google Quantum AI and Collaborators, Quantum error correction below the surface code threshold, *Nature* **638**, 920 (2025).
 - [14] N. Lacroix, A. Bourassa, F. J. H. Heras, L. M. Zhang, J. Bausch, A. W. Senior, T. Edlich, N. Shutty, V. Sivak, A. Bengtsson, M. McEwen, O. Higgott, D. Kafri, *et al.*, Scaling and logic in the colour code on a superconducting quantum processor, *Nature* **645**, 614 (2025).
 - [15] A. Eickbusch, M. McEwen, V. Sivak, A. Bourassa, J. Atalaya, J. Claes, D. Kafri, C. Gidney, C. W. Warren, *et al.*, Demonstration of dynamic surface codes, *Nature Physics* [10.1038/s41567-025-03070-w](https://doi.org/10.1038/s41567-025-03070-w) (2025).
 - [16] Z. Ni, S. Li, X. Deng, Y. Cai, L. Zhang, W. Wang, Z.-B. Yang, H. Yu, F. Yan, S. Liu, C.-L. Zou, L. Sun, S.-B. Zheng, Y. Xu, and D. Yu, Beating the break-even point with a discrete-variable-encoded logical qubit, *Nature* **616**, 56 (2023).
 - [17] V. V. Sivak, A. Eickbusch, B. Royer, S. Singh, I. Tsioutsios, S. Ganjam, A. Miano, B. L. Brock, A. Z. Ding, L. Frunzio, S. M. Girvin, R. J. Schoelkopf, and M. H. Devoret, Real-time quantum error correction beyond break-even, *Nature* **616**, 50 (2023).
 - [18] W. P. Livingston, M. S. Blok, E. Flurin, J. Dressel, A. N. Jordan, and I. Siddiqi, Experimental demonstration of continuous quantum error correction, *Nature Communications* **13**, 2307 (2022).
 - [19] D. Ristè, M. Dukalski, C. A. Watson, G. de Lange, M. J. Tiggelman, Y. M. Blanter, K. W. Lehnert, R. N. Schouten, and L. DiCarlo, Deterministic entanglement of superconducting qubits by parity measurement and feedback, *Nature* **502**, 350 (2013).
 - [20] E. Bäumer, V. Tripathi, D. S. Wang, P. Rall, E. H. Chen, S. Majumder, A. Seif, and Z. K. Mineev, Efficient long-range entanglement using dynamic circuits, *PRX Quantum* **5**, 030339 (2024).
 - [21] F. Battistel, B. Varbanov, and B. Terhal, Hardware-efficient leakage-reduction scheme for quantum error correction with superconducting transmon qubits, *PRX Quantum* **2**, 030314 (2021).
 - [22] P. Magnard, P. Kurpiers, B. Royer, T. Walter, J.-C. Besse, S. Gasparinetti, M. Pechal, J. Heinsoo, S. Storz, A. Blais, and A. Wallraff, Fast and unconditional all-microwave reset of a superconducting qubit, *Phys. Rev. Lett.* **121**, 060502 (2018).
 - [23] S. Zeytinoglu, M. Pechal, S. Berger, A. A. Abdumalikov, A. Wallraff, and S. Filipp, Microwave-induced amplitude- and phase-tunable qubit-resonator coupling in circuit quantum electrodynamics, *Phys. Rev. A* **91**, 043846 (2015).
 - [24] D. Egger, M. Werninghaus, M. Ganzhorn, G. Salis, A. Fuhrer, P. Müller, and S. Filipp, Pulsed reset protocol for fixed-frequency superconducting qubits, *Phys. Rev. Appl.* **10**, 044030 (2018).
 - [25] J. Heinsoo, C. K. Andersen, A. Remm, S. Krinner, T. Walter, Y. Salathé, S. Gasparinetti, J.-C. Besse, A. Potočník, A. Wallraff, and C. Eichler, Rapid high-fidelity multiplexed readout of superconducting qubits, *Phys. Rev. Appl.* **10**, 034040 (2018).
 - [26] E. Jeffrey, D. Sank, J. Y. Mutus, T. C. White, J. Kelly, R. Barends, Y. Chen, Z. Chen, B. Chiaro, A. Dunsworth, A. Megrant, P. J. J. O'Malley, C. Neill, P. Roushan, A. Vainsencher, J. Wenner, A. N. Cleland, and J. M. Martinis, Fast accurate state measurement with superconducting qubits, *Phys. Rev. Lett.* **112**, 190504 (2014).
 - [27] M. D. Reed, B. R. Johnson, A. A. Houck, L. DiCarlo, J. M. Chow, D. I. Schuster, L. Frunzio, and R. J. Schoelkopf, Fast reset and suppressing spontaneous emission of a superconducting qubit, *Applied Physics Letters* **96**, 203110 (2010).
 - [28] S. Boutin, C. K. Andersen, J. Venkatraman, A. J. Ferris, and A. Blais, Resonator reset in circuit qed by optimal control for large open quantum systems, *Phys. Rev. A* **96**, 042315 (2017).
 - [29] D. T. McClure, H. Paik, L. S. Bishop, M. Steffen, J. M. Chow, and J. M. Gambetta, Rapid driven reset of a qubit readout resonator, *Phys. Rev. Appl.* **5**, 011001 (2016).
 - [30] M. Göppl, A. Fragner, M. Baur, R. Bianchetti, S. Filipp, J. M. Fink, P. J. Leek, G. Puebla, L. Steffen, and A. Wallraff, Coplanar waveguide resonators for circuit quantum electrodynamics, *Journal of Applied Physics* **104**, 113904 (2008).
 - [31] M. J. Collett and C. W. Gardiner, Squeezing of intracavity and traveling-wave light fields produced in parametric amplification, *Phys. Rev. A* **30**, 1386 (1984).
 - [32] C. W. Gardiner and M. J. Collett, Input and output in damped quantum systems: Quantum stochastic differential equations and the master equation, *Phys. Rev. A* **31**, 3761 (1985).
 - [33] B. Yurke and J. S. Denker, Quantum network theory, *Phys. Rev. A* **29**, 1419 (1984).
 - [34] J. Gambetta, A. Blais, D. I. Schuster, A. Wallraff, L. Frunzio, J. Majer, M. H. Devoret, S. M. Girvin, and R. J. Schoelkopf, Qubit-photon interactions in a cavity: Measurement-induced dephasing and number splitting, *Phys. Rev. A* **74**, 042318 (2006).
 - [35] J. Koch, T. M. Yu, J. Gambetta, A. A. Houck, D. I. Schuster, J. Majer, A. Blais, M. H. Devoret, S. M. Girvin, and R. J. Schoelkopf, Charge-insensitive qubit design derived from the cooper pair box, *Phys. Rev. A* **76**, 042319 (2007).

- (2007).
- [36] M. Boissonneault, J. M. Gambetta, and A. Blais, Non-linear dispersive regime of cavity qed: The dressed dephasing model, *Phys. Rev. A* **77**, 060305 (2008).
 - [37] M. Boissonneault, J. M. Gambetta, and A. Blais, Improved superconducting qubit readout by qubit-induced nonlinearities, *Phys. Rev. Lett.* **105**, 100504 (2010).
 - [38] M. D. Reed, L. DiCarlo, B. R. Johnson, L. Sun, D. I. Schuster, L. Frunzio, and R. J. Schoelkopf, High-fidelity readout in circuit quantum electrodynamics using the jaynes-cummings nonlinearity, *Phys. Rev. Lett.* **105**, 173601 (2010).
 - [39] D. I. Schuster, A. Wallraff, A. Blais, L. Frunzio, R.-S. Huang, J. Majer, S. M. Girvin, and R. J. Schoelkopf, ac stark shift and dephasing of a superconducting qubit strongly coupled to a cavity field, *Phys. Rev. Lett.* **94**, 123602 (2005).
 - [40] D. Sank, Z. Chen, M. Khezri, J. Kelly, R. Barends, B. Campbell, Y. Chen, B. Chiaro, A. Dunsworth, A. Fowler, E. Jeffrey, E. Lucero, A. Megrant, J. Mutus, M. Neeley, C. Neill, P. J. J. O'Malley, C. Quintana, P. Roushan, A. Vainsencher, T. White, J. Wenner, A. N. Korotkov, and J. M. Martinis, Measurement-induced state transitions in a superconducting qubit: Beyond the rotating wave approximation, *Phys. Rev. Lett.* **117**, 190503 (2016).
 - [41] M. Khezri, A. Opremcak, Z. Chen, K. C. Miao, M. McEwen, A. Bengtsson, T. White, O. Naaman, D. Sank, A. N. Korotkov, Y. Chen, and V. Smelyanskiy, Measurement-induced state transitions in a superconducting qubit: Within the rotating-wave approximation, *Phys. Rev. Appl.* **20**, 054008 (2023).
 - [42] M. F. Dumas, B. Groleau-Paré, A. McDonald, M. H. Muñoz Arias, C. Lledó, B. D'Anjou, and A. Blais, Measurement-induced transmon ionization, *Phys. Rev. X* **14**, 041023 (2024).
 - [43] R. Shillito, A. Petrescu, J. Cohen, J. Beall, M. Hauru, M. Ganahl, A. G. Lewis, G. Vidal, and A. Blais, Dynamics of transmon ionization, *Phys. Rev. Appl.* **18**, 034031 (2022).
 - [44] K. N. Nesterov and I. V. Pechenezhskiy, Measurement-induced state transitions in dispersive qubit-readout schemes, *Phys. Rev. Appl.* **22**, 064038 (2024).
 - [45] T. Connolly, P. D. Kurilovich, V. D. Kurilovich, C. G. L. Bøttcher, S. Hazra, W. Dai, A. Z. Ding, V. R. Joshi, H. Nho, S. Diamond, D. K. Weiss, V. Fatemi, L. Frunzio, L. I. Glazman, and M. H. Devoret, [Full characterization of measurement-induced transitions of a superconducting qubit](#) (2025), [arXiv:2506.05306 \[quant-ph\]](#).
 - [46] W. Dai, S. Hazra, D. K. Weiss, P. D. Kurilovich, T. Connolly, H. K. Babla, S. Singh, V. R. Joshi, A. Z. Ding, P. D. Parakh, J. Venkatraman, X. Xiao, L. Frunzio, and M. H. Devoret, [Spectroscopy of drive-induced unwanted state transitions in superconducting circuits](#) (2025), [arXiv:2506.24070 \[quant-ph\]](#).
 - [47] T. Thorbeck, Z. Xiao, A. Kamal, and L. C. G. Govia, Readout-induced suppression and enhancement of superconducting qubit lifetimes, *Phys. Rev. Lett.* **132**, 090602 (2024).
 - [48] M. Malekakhlagh, A. Petrescu, and H. E. Türeci, Lifetime renormalization of weakly anharmonic superconducting qubits. i. role of number nonconserving terms, *Phys. Rev. B* **101**, 134509 (2020).
 - [49] A. Petrescu, M. Malekakhlagh, and H. E. Türeci, Lifetime renormalization of driven weakly anharmonic superconducting qubits. ii. the readout problem, *Phys. Rev. B* **101**, 134510 (2020).
 - [50] Z. Chen, J. Kelly, C. Quintana, R. Barends, B. Campbell, Y. Chen, B. Chiaro, A. Dunsworth, A. G. Fowler, E. Lucero, E. Jeffrey, A. Megrant, J. Mutus, M. Neeley, C. Neill, P. J. J. O'Malley, P. Roushan, D. Sank, A. Vainsencher, J. Wenner, T. C. White, A. N. Korotkov, and J. M. Martinis, Measuring and suppressing quantum state leakage in a superconducting qubit, *Phys. Rev. Lett.* **116**, 020501 (2016).
 - [51] C. Wang, M.-C. Chen, C.-Y. Lu, and J.-W. Pan, Optimal readout of superconducting qubits exploiting high-level states, *Fundamental Research* **1**, 16 (2021).
 - [52] Z. Wang, B. D'Anjou, P. Gigon, A. Blais, and M. S. Blok, [Probing excited-state dynamics of transmon ionization](#) (2025), [arXiv:2505.00639 \[quant-ph\]](#).
 - [53] P. Duan, Z. Jia, C. Zhang, L. Du, H. Tao, X. Yang, L. Guo, Y. Chen, H. Zhang, Z. Peng, W. Kong, H.-O. Li, G. Cao, and G.-P. Guo, Broadband flux-pumped josephson parametric amplifier with an on-chip coplanar waveguide impedance transformer, *Applied Physics Express* **14**, 042011 (2021).